

Directly Deposited Binder Free Sulfur Electrode Enabled by Air-Controlled Electrospray Process

Willy Halim, Jin-Hong Lee, Sang-Mok Park, Rui Zhang, Snatika Sarkar, Travis O'Neil, Yi-Chen Chiang, and Yong Lak Joo*

Robert Frederick Smith School of Chemical and Biomolecular Engineering, Cornell University, Ithaca, NY, 14853, USA

*Corresponding author E-mail address: ylj2@cornell.edu (Y.L. Joo)

Abstract

Lithium-sulfur batteries are one of the most promising energy storage technologies to replace commercial Li-ion batteries due to five-fold higher theoretical energy density, and lower cost. However, due to certain limitations, the technology is not ready to be deployed. To overcome some of these, scientists have been extensively employing graphene oxide (GO) or graphene material to improve the electrochemical performance. In this work, we present a unique, novel, and facile method to deposit the active materials onto an aluminum collector by utilizing the Van der Waals interaction between graphene oxide and aluminum via an air-controlled electrospray (ACES) process. The role of conventional polymer binder was replaced by graphene, resulting in a binder-free substrate. We demonstrated that the elimination of conventional polymer binder and graphene layers assembled via the ACES method resulted in higher capacity and retention, and offer almost four times higher capacity at 2C than the conventional slurry-cast system with polymer binder. This ACES technique offers potential for improving the overall energy density of sulfur and being adapted for commercialization in the energy storage industry.

Keywords: Binder-free; air-controlled electrospray; graphene oxide; graphene; lithium-sulfur battery

1. Introduction

Due to the rapid development of electronics and electric vehicles, it is imperative to develop new technology for energy storage applications. Lithium-sulfur (Li-S) is one of the promising candidates for energy storage applications because it possesses high theoretical capacity and energy density at 1,670 mAh g⁻¹ and 2,500 kW kg⁻¹, respectively¹⁻³. Also, the low cost and environmentally benign nature of sulfur components are attractive from an economic and environmental perspective^{4,5}. Despite these advantages, several obstacles persist that hinder the commercialization of lithium-sulfur technology. For example, expansion and contraction of active

materials during the discharge/charge process, rapid capacity fading due to polysulfide migration, and insulating properties of the sulfur material itself⁶⁻⁸.

Many approaches have been conducted to circumvent the problems by improving electrical conductivity and trapping the polysulfide species. The most popular approach is employing carbonaceous material, such as: bimodal mesoporous carbon⁹⁻¹¹, carbon nanotubes¹²⁻¹⁴, conductive polymer like carbon nanofiber¹⁵⁻¹⁸, PEDOT:PSS^{19,20}, graphene oxide (GO)^{21,22}, and graphene materials within the cathode itself²³⁻²⁵. In this last approach, embedding interlayers or applying surface modification is very useful for high sulfur loading^{16,18,26}. Addition of GO is one of the most popular methods due to its ability to capture polysulfide by acting as a physical barrier, and also through chemisorption by polar-polar interactions. Binding between oxygen functional groups and sulfur polysulfide has been proven to maintain high capacity retention^{22,23,27-31}. However, researchers often overlook another potential attribute of graphene oxide. Most of the current literature focuses on utilizing the oxide content to capture polysulfide as opposed to using GO's other efficacies to anchor active materials onto the aluminum electrode.

In 2015, layer by layer reduced graphene oxide (rGO) deposition onto the aluminum electrode by an electro spray method was reported^{32,33}. The binding interaction between GO/rGO and aluminum oxide layer was further asserted using density functional theory³⁴. These ideas inspired us to develop an advanced technique to deposit graphene oxide and active sulfur materials simultaneously. Previously, we successfully implemented our novel air-controlled electro spray (ACES) technique for Li-ion batteries and high loading sulfur in Li-S technology^{16,35}. This approach permits coating of diverse materials on various surfaces. Herein, we present a novel, facile, and scalable method of the deposition process that utilizes GO as a binder and polysulfide anchor. In general, our electrode fabrication method is only a two-step process: ACES followed by heat treatment. In this manner, we were able to achieve sulfur deposition on aluminum collector without conventional polymer adhesive. In addition, the quick dry spray process

eliminates the cracking that results from a typical drying method ³⁶. As for the conductive carbon, we implemented commercial Ketjen Black with pulverized mesoporous carbon nanofiber (MPCNF) and GO. The overall concentration of GO was less than 1%. To further improve the electrochemical performance of the cell, we also replaced the binder content with commercially available graphene solution to promote electron pathways and sulfur utilization. Incorporation of graphene in the electrode was carried out with the ACES process (ACES-Gr)

For the reference system, a conventional slurry coated electrode with binder was prepared. We utilized lithium polyacrylate (LiPAA) as a polymer binder because LiPAA has shown the best performance among polyvinylidene fluoride (PVDF), polyvinylpyrrolidone (PVP), polyethylene imine (PEI), PVP:PEI (5:1), and Polyaniline (PANI) ³⁷. The composition of variables of interest is summarized in Table 1 below.

Table 1. Summary of the cathode composition with different approach

Process	Sulfur (%)	Carbon Composite – Ketjen Black : MPCNF+rGO (1:1) weight ratio (%)	Binder LiPAA (%)	Graphene (%)
Conventional slurry coating method (SC)	56	34	10	0
Air-controlled electro spray method (ACES)	56	44	0	0
Air-controlled electro spray method (ACES-Gr)	56	34	0	10

2. Experimental

2.1 Fabrication of MPCNF+GO powder

1.2 g of polyacrylonitrile (PAN, MW = 150,000, Sigma Aldrich), 0.8 g of polymethylmethacrylate (PMMA) (MW = 15,000 Sigma Aldrich), 0.3 g of tetraethyl orthosilicate (TEOS) (Reagent Grade, Sigma Aldrich), and 0.05 g of Zinc Chloride (ZnCl_2) (Reagent Grade, Amresco) were dissolved in 12 mL of dimethylformamide (DMF) (Alfa Cesar) to form 13.7 wt % of polymer content. The solution was stirred for 72 hours at 65°C to enhance polymer crosslinking. Air-controlled electrospinning was used to spin 6 ml of the polymer solution with a PHD 2000 Infusion syringe pump (Harvard Apparatus) and a coaxial needle at room temperature. The solution was supplied to the inner 12-gauge needle, and 12 psi air flow rate was applied through the 17-gauge outer shell. The distance between the nozzle tip and aluminum current collector was 30 cm. Positive potential 15 kV was induced to the outer nozzle, and solution feeding rate was set at 0.1 ml min⁻¹. The resulting fiber was peeled and folded to 4 X 6 inches for heat treatment. Initially, the fiber was subjected to stabilization at 280°C for 2 hours under stagnant air with a ramp rate of 5°C min⁻¹, followed by carbonization at 900°C for 2 hours with a ramp rate of 5°C min⁻¹ under N₂ flow, and finally activation at 900°C for 2 hours with a ramp rate of 5°C min⁻¹ under CO₂ flow.

Commercial graphene oxide solution (Dongjin Semichem) was diluted with distilled water to 6 mg ml⁻¹. Then, 5 ml of the solution was extracted and sprayed onto activated MPCNF substrate using ACES method. The positive potential was applied at 25 kV, the distance between the nozzle tip to the collector was 30 cm, solution feeding rate was set at 0.1 ml min⁻¹, and 20 psi airflow was applied through the outer stainless-steel nozzle. After spraying, the surface color of the MPCNF turned into a dark grey, indicating successful coating of GO on MPCNF. Finally, the obtained MPCNF coated GO sheets were pulverized using a ball mill for 15 minutes to form a fine powder.

2.2 Preparation of Slurry Coated Electrode (SC)

Initially, 0.56 g of active sulfur material (Spectrum Chemical) was mixed with 0.17 g of Ketjen Black (AkzoNobel) and 0.17 g of MPCNF+GO powder. Then, the mixture was heat treated under air at 155°C for 12 hours to ensure sulfur infiltration and simultaneously reduce the graphene oxide. LiPAA was synthesized by mixing 5 wt % of a polyacrylic acid (PAA) (MW = 450,000, Sigma Aldrich) in H₂O solution and 5 wt % of a 1:1 lithium hydroxide (LiOH) (Powder, Reagent Grade Sigma Aldrich) in H₂O solution and stirred it overnight as previously reported³⁸. Then, 0.1 g of the LiPAA solution was thoroughly mixed with the sulfur-carbon composites in a ball mill for 10 minutes. The slurry paste was then cast onto a carbon coated aluminum electrode.

2.3 Preparation of Sulfur-Carbon Solution without Graphene (AC)

Active sulfur material, Ketjen Black, and MPCNF+GO powder were mixed and heat treated as reported above. Afterward, the mixture was dissolved in a water and isopropanol solvent (8:2 weight ratio) at a concentration of 10 mg ml⁻¹.

2.4 Preparation of Sulfur-Carbon Solution with Graphene (AC-Gr)

A mixture of active sulfur material, Ketjen Black, and MPCNF+GO powder was prepared and heat treated as previously stated. Afterward, 2.5 g of commercial 4% wt graphene solution (ACS Material) is added to the mixture. Finally, the mixture is dissolved in 10 ml water and isopropanol solvent at 8:2 ratio.

2.5 Active Materials Deposition

Similarly, 10mL of sulfur-carbon solution (with or without graphene) was sprayed onto the aluminum current collector using the ACES process. The voltage applied was 25 kV, distance from the nozzle tip to current collector was 15 cm, convective airflow rate was 25 psi, and solution pump rate was 0.1 ml min⁻¹. After all the dry solutions were deposited onto the aluminum collector, the electrode was punched into 1.5 cm diameter disks. Typical active sulfur loading was around 1 mg cm⁻².

2.6 Electrolyte Composition

The electrolyte was 1 M of bis(trifluoromethane)sulfonimide lithium salt (LiTFSI) and 0.1 M of lithium nitrate (LiNO_3) in a 1:1 volume ratio of 1,2-dimethoxyethane (DME) and 1,3-Dioxolane (DOL). All were purchased from Sigma Aldrich. E/S ratio that we used in this experiment was 10 mL g^{-1}

2.7 Characterization Methods

Fourier Transform Infrared Spectra were recorded with a Bruker Vertex V80V Vacuum FTIR system using an average of 64 scans with a resolution of 4 cm^{-1} . Thermogravimetric analysis was carried out with a TA Instruments Q500 at a heating rate of $10 \text{ }^\circ\text{C min}^{-1}$ under an N_2 atmosphere. X-ray diffraction analysis was conducted with a Bruker D8 Advance ECO powder diffractometer from 5° to 60° at a scan rate of 0.1° s^{-1} . Scanning electron microscopy (SEM) images and energy dispersive X-ray spectroscopy (EDS) mapping were taken using an LEO 1550 FESEM. X-ray photoelectron spectroscopy measurements were conducted with a Surface Science instrument equipped with a monochromatic Al $\text{K}\alpha$ X-ray source (1468.6 eV). Electrochemical characterizations of the coated separator were performed using 2032-type coin cells consisting of Li metal anode (MTI Corporation). All cells were assembled in an argon-filled glove box. Cyclic voltammetry and electrochemical impedance spectroscopy (EIS) test were performed using a potentiostat (Princeton PARSAT 4000). Galvanostatic charge/discharge cycles were carried out in the voltage range of 1.8-2.8 V using a battery cycler (MTI Corporation) at room temperature. All current densities and specific discharge capacities calculated in this study were based on sulfur mass.

3. Results and Discussion

3.1 Heat Treatment Sulfur Encapsulation

Heat treatment at 155 °C is purported to encapsulate the sulfur inside the carbon composite, as shown in previous literature ^{39,40}. The GO content is only around 1% of the overall composition, which is essential to ensure that the insulating properties of GO do not hinder electron pathways. To confirm that there are no chemical reactions between sulfur and carbon composites after heat treatment in the system, we conducted high-resolution spectra of XPS and FTIR (Figure S1). Stagnant peaks before and after heat treatment from XPS shows that no chemical interaction happens between terminal sulfur and oxygen group from GO ⁴¹. From FTIR results, no distinct peak is formed after thermal treatment, which also clarifies the absence of chemical reaction during sulfur infusion ²¹. Wide-angle XRD patterns in Fig 1. show a sharp peak for sulfur components around 23°. Carbon composite (MPCNF + GO + KB) displays several small peaks from 8° to 60°. The absence of a peak at 10° two theta shows that the content of GO is insignificant in the system ⁴². After mixing the sulfur with the carbon composite for air-controlled electrospray (ACES), their respective peaks were observed on a single spectrum. After the heat treatment for sulfur infusion, the sharp peak at 23° disappears, implying that the bulk of sulfur crystallinity turns into amorphous sulfur. Moreover, when graphene is incorporated to the ACES system (ACES-Gr), a sharp peak at 27° is observed, indicating the presence of graphitic layer in the system ⁴³.

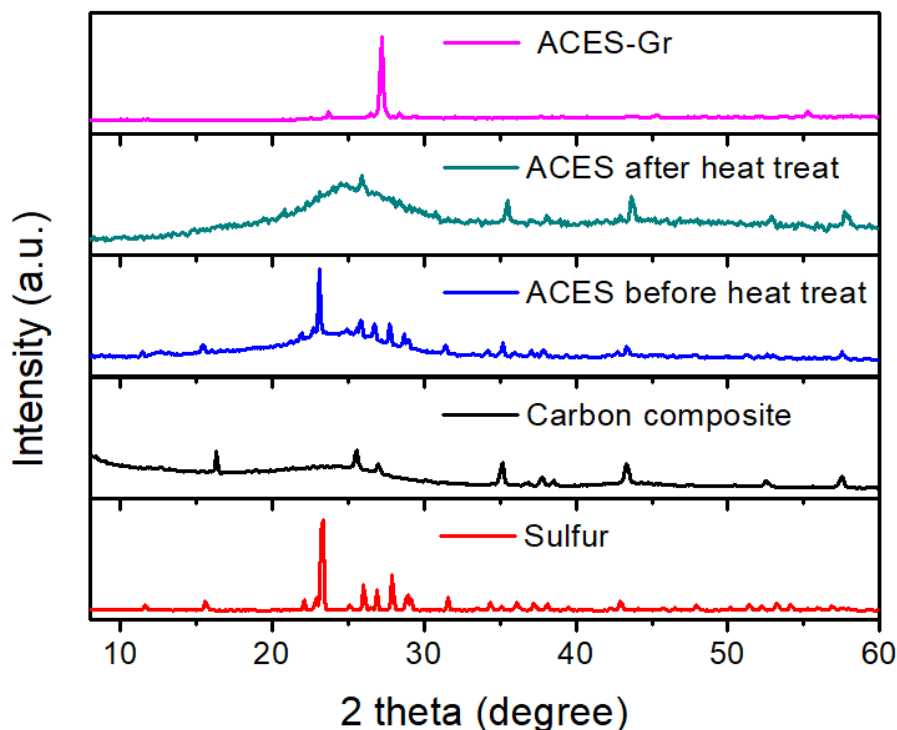


Figure 1) XRD characterization of pristine sulfur and carbon composite, then a mixture of sulfur and carbon composite before and after heat treatment, and the presence of graphene in the system.

3.2 Air Controlled Electrospray Process

The schematic process of air-controlled electrospray and conventional electrospray are illustrated in Figure 2a and c below. As opposed to conventional electrospray process, the air-controlled electrospray (ACES) utilizes a convective air flow jet to accelerate the drying and deposition process. The nozzle is comprised of two concentric cylinders. The solution is ejected from the inner cylinder, while the air propels through outer nozzle, which is connected to a high voltage source. Our studies indicate that the impinging dry air of the air-controlled electrospray process tends to form smaller charged droplets and evaporate solvent faster, resulting in dry solute deposited on the current collector. The evaporation is accelerated due to higher surface area exposed to the surrounding dry air. In general, a higher voltage, faster airflow rate, and longer

distance between the nozzle tip and current collector enhance the evaporation rate and reduce the droplet sizes of the solution. If evaporation rate is too slow, wet solutions are formed on the current collector, which cause poor particle dispersion and may disrupt uniformity. However, if evaporation rate is too fast, solutes might disappear along with the solvent, causing discontinuity and disorder in the material on the current collector. Images of the air-controlled sprayed electrode without (ACES) and with graphene (ACES-Gr) is displayed in Figure 2b & d below. Poor dispersion and non-uniform deposition are observed from the conventional electro spray process, whereas a smooth and continuous film is attained with the air-controlled electro spray process. After the ACES process finishes, the electrochemical performance of the resulting dry solutes can be tested immediately, contrary to solution casting that requires additional drying. This also makes ACES an effective method for scaling up. Image of the actual ACES process is displayed in Figure S2. The deposition is presumably enabled by the interaction between charged graphene oxide and an aluminum oxide film on the current collector as mentioned in previous reports^{33,34}.

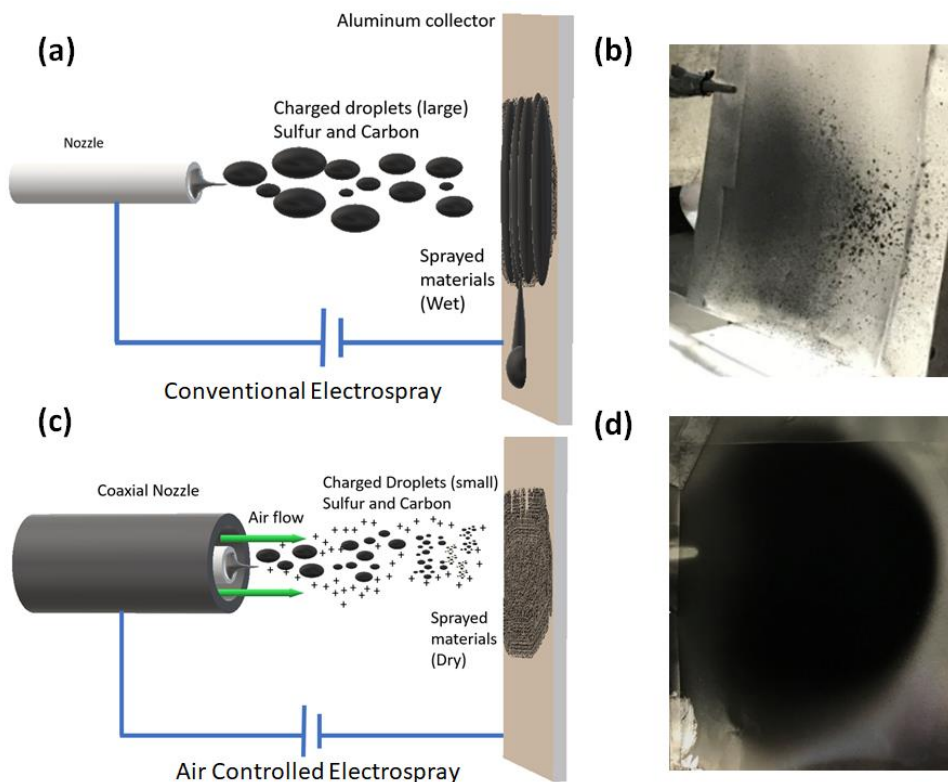


Figure 2 Schematic illustration and photo image of sprayed material on a collector of conventional electrospray (a and b) and air-controlled electrospray (ACES) (c and d).

3.3 Surface Morphology and Characterization.

The morphologies between conventional slurry coating (SC) and ACES can be easily distinguished from SEM images (Fig 3). Top view and cross-sectional images of the SC technique (Fig. 3a-b) show a dense and smooth film with cracking. This inevitable cracking happens during the drying process. The fracture amplifies as the sulfur loading increases ³⁶. By looking at the cross-sectional images, the cracking only appears on the surface. An intact structure is observed beneath the surface, which is presumably due to low sulfur loading. However, in the ACES technique (Fig. 3c-d), voids and rough surfaces are observed while carbon interconnections are preserved. A porous morphology is beneficial to the sulfur electrode as it accommodates the sulfur expansion during cycling to preserve the structure ⁴⁴. Moreover, it also provides good accessibility of electrolyte to active sulfur materials. In the SC method, uniform thickness and smooth surfaces are maintained because a fixed gap is applied from the doctor blade. In ACES process, thickness is a function of flow rate, distance, and convective airflow. These factors make it extremely difficult to produce a flat, smooth, and continuous structure. Despite the difference in morphology, sulfur and carbon are uniformly well-dispersed for both systems as depicted in EDS (central images of Fig. 3). In most electrochemical systems, uniform state of the electrode is a crucial factor in obtaining consistent and accurate results.

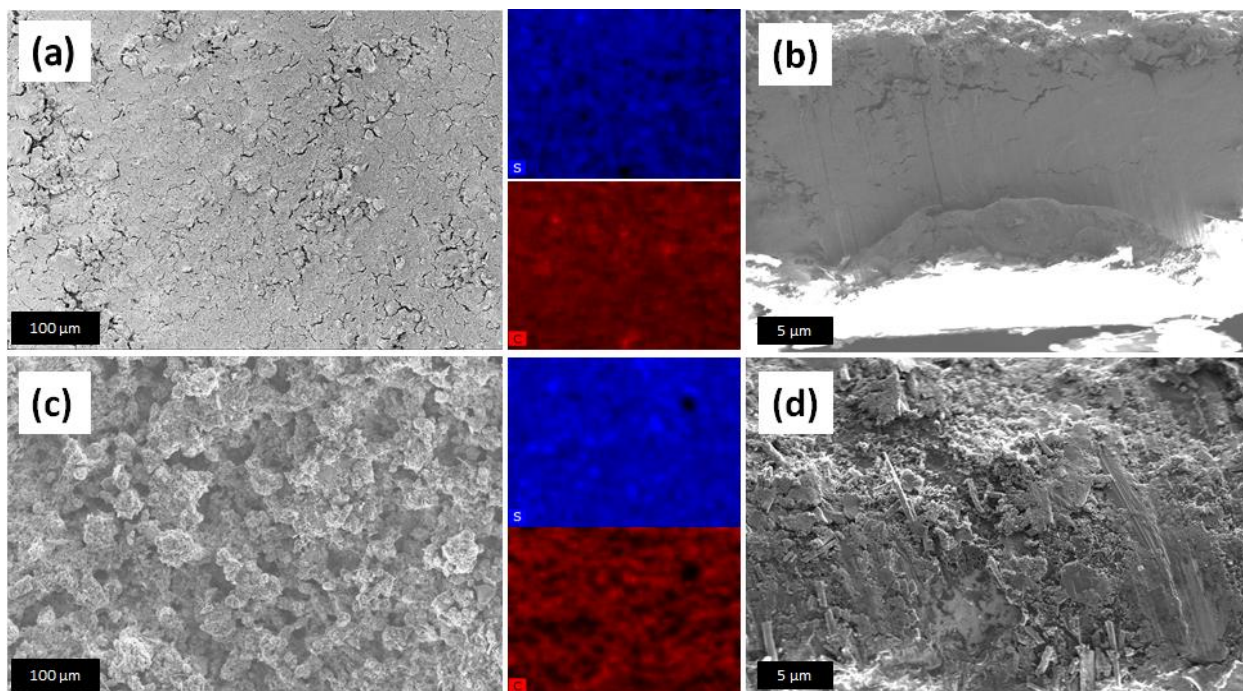


Figure 3. SEM images of top view and cross section of sulfur-carbon composite prepared by SC (a and b) and ACES (c and d). EDS mapping of sulfur and carbon correspond to top view images of part a and c.

The incorporation of graphene solution results in structural changes of sulfur-carbon active materials. High-resolution SEM measurement was carried out to distinguish structural differences from the incorporation of graphene sheets. From the ACES image of Figure 4 a), it is seen that sulfur is aggregated on the carbon nanofiber substrate. In the ACES-Gr image of Figure 4 c), thin planar graphene sheets cover the surface of active materials. This encapsulation is self-assembled during the spray process.

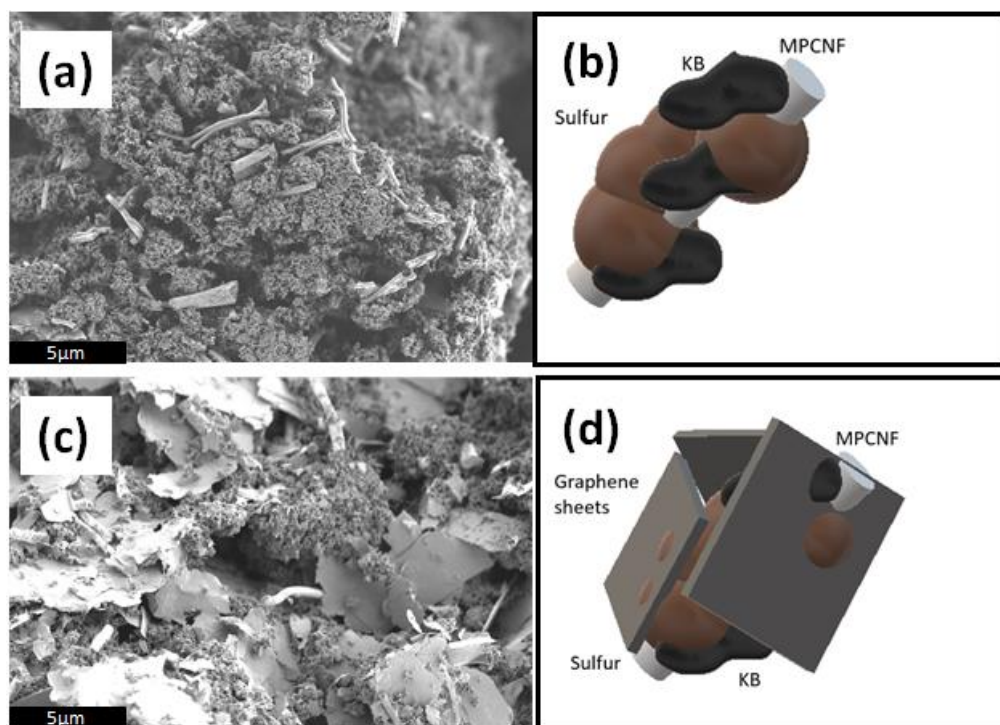


Figure 4. High magnification SEM images and schematic illustration of sulfur-carbon composite prepared by ACES (a and b) and ACES-Gr system (c and d).

3.4 Electrochemical Performance

Cyclic voltammogram (CV) profiles of SC, ACES, and ACES-Gr are displayed in Figure 5 below. Cyclic voltammetry was conducted from 2.8 V to 1.6 V at a scan rate 0.1 mV s^{-1} . Two reduction peaks are observed in all samples. The first reduction peak at around 2.2 V corresponds to the reduction of S_8 to higher order polysulfides (Li_2S_x , $4 \leq x \leq 8$), and the second reduction at 2.0 V is ascribed to a further reduction to insoluble Li_2S ^{45,46}. In the SC and ACES systems, the first reduction peak happens at around 2.2 V. After the first cycle, the peak shifted to around 2.3 V, and the second reduction peak stabilized to 2.0 V after several cycles suggesting a higher kinetic barrier for the direct reduction of bulk-sized commercial sulfur powder to polysulfides. By replacing binder with graphene sheets, the first and second reduction peaks of ACES-Gr were maintained at 2.3 V and 2.0 V for all cycles, which implies superior stability in lithium-sulfur

performance. In addition, replacing binder with graphene produces sharp reduction peak at 2.0 V, indicating excellent utilization of active materials from the sulfur-carbon network. The clear distinction can be detected from the oxidation peak between SC and ACES. The SC technique only has one peak at 2.42 V, whereas the ACES process has two oxidation peaks at 2.38 at 2.42 V after the first cycle. A singlet anodic peak at 2.4 V confirms the oxidation of insoluble polysulfide to Li_2S_8 ⁴⁶, whereas doublet anodic peak at 2.38 V and 2.42 V implies complete conversion to S_8 ⁴⁷.

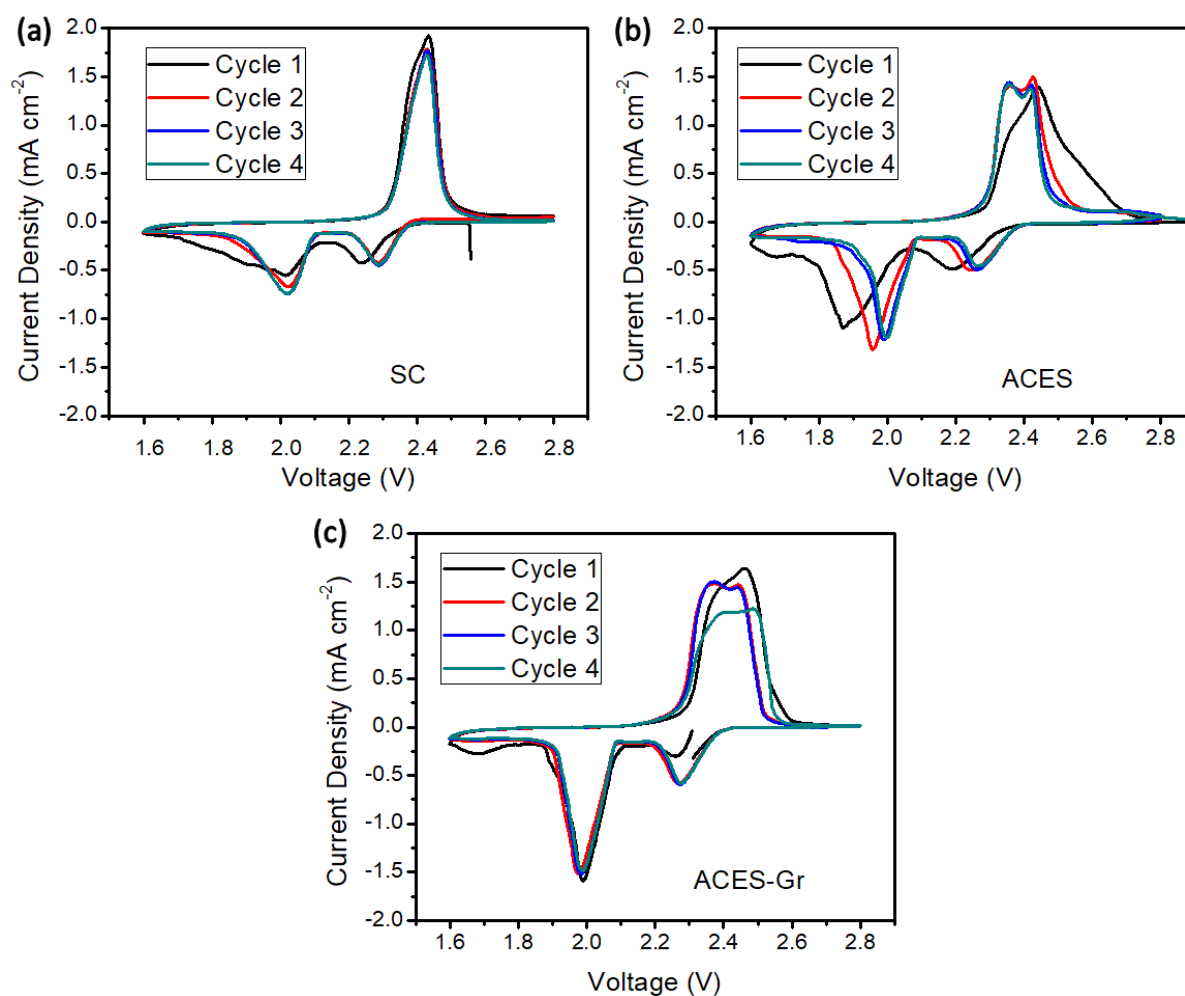


Figure 5) Cyclic voltammogram of sulfur-carbon composite prepared by various techniques a) SC b) ACES c) ACES-Gr.

To elucidate the advantage of ACES deposition, electrochemical impedance spectroscopy (EIS), cycling performance, and rate capability were carried out (Fig 6a-c). The EIS result from 10^7 Hz to 0.01 Hz at 5 mV amplitude is displayed in Figure 6a. The ACES system had a slightly shorter x-intercept and half semicircle as opposed to a conventional SC system, which suggests that the replacement of binder with carbon decreases interfacial and charge transfer resistances of the cells ⁴⁸. Then, the integration of graphene reduces the semicircle and x-intercept even further due to the excellent electrical conduit from the carbon planar. This phenomenon ensures better electrochemical environment and higher utilization of the active material, which shows an agreement with the CV data from Figure 5.

Prior to electrochemical cycling, thermogravimetric analysis (TGA) was carried out to justify that the composition of sulfur is around 56 % after the spraying process (Figure S3). To evaluate the electrochemical performance, electrodes produced by SC, ACES, and ACES-Gr with sulfur loading of 1 mg cm^{-2} were cycled from 1.8 V to 2.8 V at the C/4 rate for cyclability testing and different current densities to test rate capability (Fig 6b). At a rate of C/4, the initial capacity of 849.5 mAh g^{-1} , 926.3 mAh g^{-1} , and 1076 mAh g^{-1} are obtained for the SC, ACES, and ACES-Gr cells, respectively. The significant decay on the first few cycles was caused by excess electrolyte in the system. The excess electrolyte was purported to ensure proper wetting. However, extra electrolyte enhances PS dissolution and migration to the inactive areas within the cell where they cannot participate in further reactions. Therefore, it leads to lower active PS concentration, which shifts the equilibrium to the lower order polysulfide ⁴⁹. Improved cycling performance compared to the SC technique is clear. The ACES system delivers good capacity retention over 100 cycles at C/4 with a fade rate of 0.31% and 0.33% per cycles with and without graphene addition, whereas the SC method declines at 0.44% per cycle. Several studies have indicated that the presence of rGO increased both capacity and retention significantly. In this report, only a minuscule amount of rGO was implemented, which acted as a

binder and polysulfide suppressor. Thus, the amount added may not be sufficient to raise the performance significantly as previously shown. It is believed that the moderate increase of performance is mainly due to the porous cathode structure that enhances electrolyte wetting and reaction site availability^{50,51}.

The cells from the ACES system also display remarkable discharge capacity at a higher rate. They are discharged/charged at various current densities from C/10 to 2C for five cycles at each rate. The results show that as the rate increases, the difference of discharge capacity becomes more apparent. By replacing insulating binder with more electrically conductive carbon, the reversible capacity is increased from 142 mAh g⁻¹ to 348 mAh g⁻¹ at 2C discharge rate. Moreover, by integrating graphene sheets into the cell, the reversible capacity is further improved to 550 mAh g⁻¹ at 2C. This shows that electron pathway and lithium-ion accessibility are critical in achieving remarkable capacity at higher current. Overall, the ACES system achieves higher discharge capacity due to favorable kinetics from higher electronic conductivity and excellent electrolyte accessibility because of the rough and porous cathode structure.

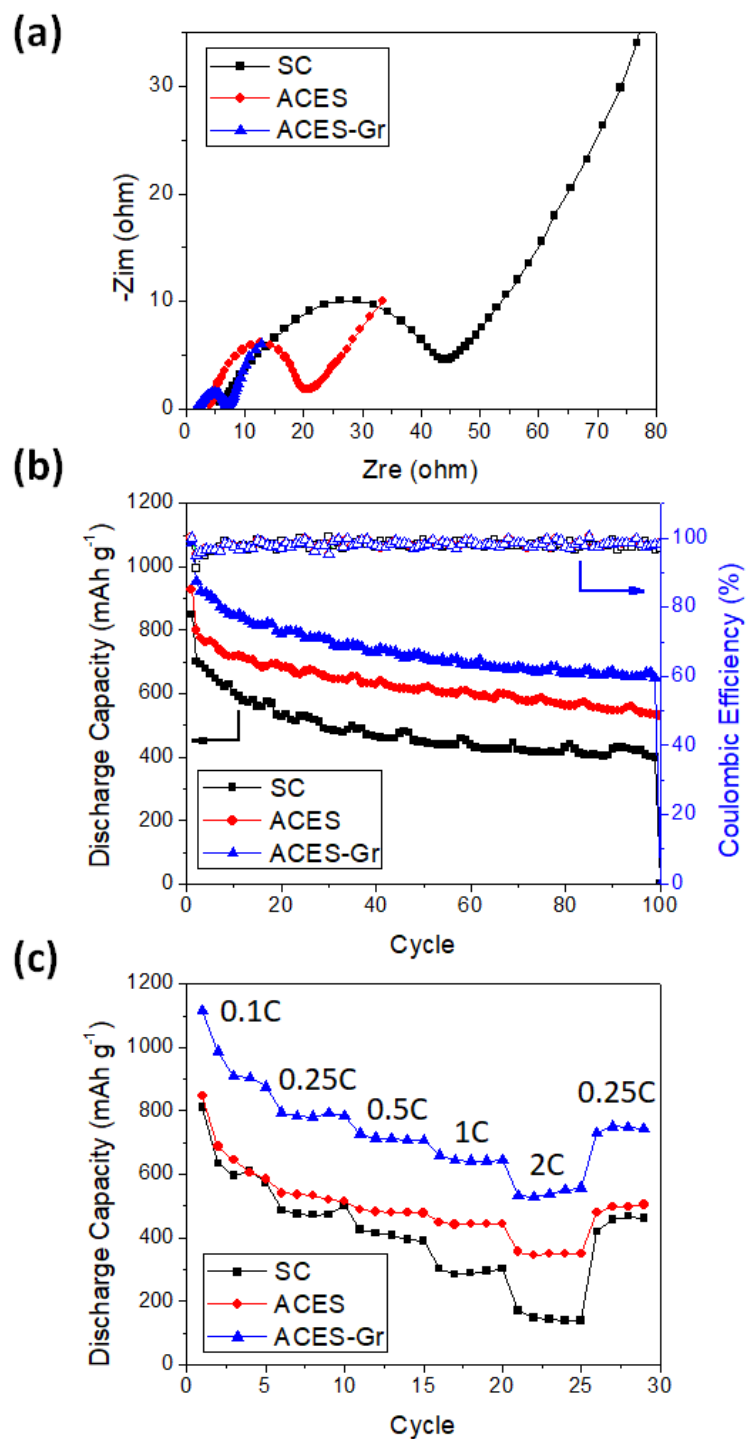


Figure 6 a) Impedance spectra b) cycling performance at 0.25C rate ($1C = 1670 \text{ mA g}^{-1}$) and c) rate capability of sulfur-carbon composite prepared by various deposition methods.

3.5 Post-Mortem Analysis

After the cell finished cycling, we conducted SEM and high-resolution S_{2p} spectra to investigate morphologies and polysulfide profiles (Fig. 7a,c,e). The SEM images show that the number of rifts increased, the gaps widened, and particles aggregated more. These presumably occur during continuous discharge and charge because the compact structure does not accommodate volume expansion. The expansion induces constant stress among neighboring particles during the discharge/charge process, resulting in cracking and more structure disorder. Surprisingly, the ACES structure becomes more compact after 100 cycles of charge/discharge process. The pores are filled with sulfur-carbon composite. Cracking is observed after cycling, but less apparent and ubiquitous compared to the conventional slurry coating process. As for graphene incorporated electrode, the structure is completely intact and coarse, which indicates excellent trapping of polysulfide species. A clear distinction of morphology at various resolutions before and after cycling is displayed in Figure S4.

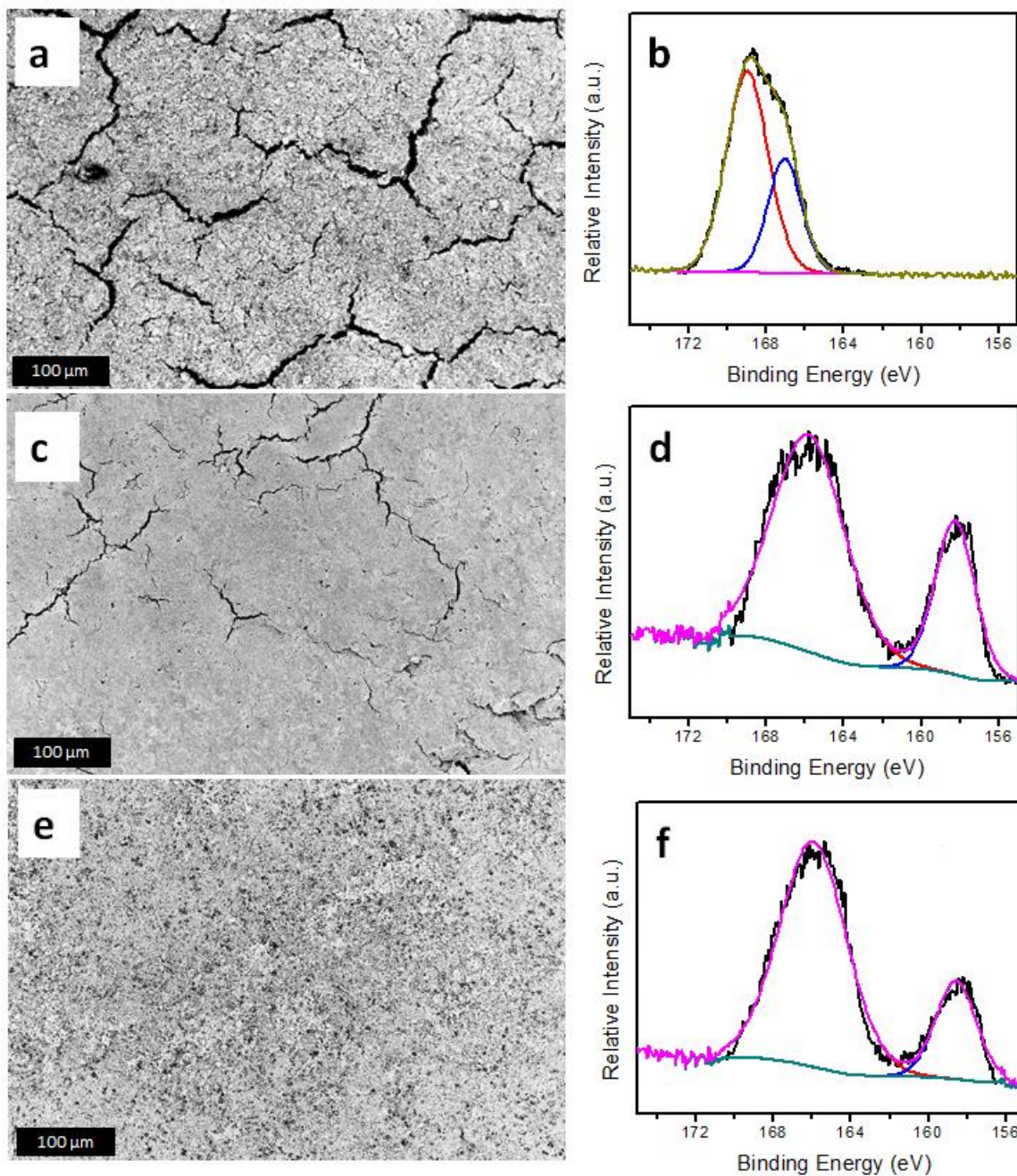


Figure 7) SEM images of sulfur cathode after cycling from a) SC c) ACES e) ACES-Gr. High-resolution S_{2p} of sulfur cathode after cycling from b) SC d) ACES f) ACES-Gr.

We conducted high-resolution S_{2p} spectra after finished cycling to probe the effect of the ACES process (Fig. 7b,d,f). Surprisingly, both the ACES and ACES-Gr exhibit two peaks at

around 165.7 and 158.4 eV, whereas the SC process only displays one sharp peak at 168.7 eV with a shoulder on the right-hand side at 166.9 eV. The peaks at 165.7 eV can be attributed to sulfonyl residue from the LiTFSI salt and sulfur oxide species from electrolyte decomposition, and the peak at 158.4 eV corresponds to insoluble polysulfides, Li_2S_2 and Li_2S ^{52,53}. Absence of the second peak from SC technique entails the possibility that lithium polysulfide completely detached and migrated to the lithium anode.

The SEM images and EDS mapping on lithium anodes confirm the migration of polysulfide onto the lithium surface (Figure S5). In the SC system, the lithium anode surface shows intense cracking and polysulfide coverage. However, in the ACES system, fewer bulk polysulfides are deposited on the anode, suggesting that morphology is important in suppressing the migration of polysulfide. Moreover, the ACES-Gr system displays significantly less number of particles and sulfur distribution as observed in the EDS spectra. From this outcome, we speculate that rough morphology has a beneficial role in inhibiting the polysulfide shuttle effect. As the tortuosity increases from surface area roughness, the path for polysulfides to the anode side is delayed, and they are ultimately trapped inside the carbon composites structures. Also, the encapsulation of sulfur by a graphene composite adds an extra barrier for the diffusion of soluble sulfur to the anode side, which causes significantly less insoluble polysulfide deposited onto the lithium anode.

Lastly, we conducted EIS measurements to observe the increase in charge transfer resistance after cycling (Figure S6). After 100 cycles, the width of the semicircle of the cell prepared by SC method doubled, whereas the cells made by ACES and ACES-Gr only increased by less than 25%. This phenomenon corresponds to lithium passivation by the shuttle effect and provides an agreement with the SEM, EDS, and high resolution XPS spectra. The significant increase in cell resistance resulted from the high frequency of lithium polysulfides deposited on the lithium surface. Lower amounts of lithium polysulfides on the lithium of ACES and ACES-Gr cells minimized surface passivation and the increase in charge transfer resistance.

These results suggest that an inherent cathode structural configuration also influences the lithium-sulfur electrochemical performance and shuttling effect. For the SC system, a more compact cathode structure explains lower sulfur utilization because less active materials are exposed to the electrolyte, and the soluble polysulfides that form on the interfacial surface tend to escape easily from the cathodes. However, for the ACES system, greater accessibility of electrolyte and sulfur particles ensures higher active material utilization and better retention due to more sulfur particles reacting with lithium ions. Greater tortuosity interferes with the polysulfide migration to the lithium anode.

As the ACES system introduces binder free and a unique morphology, it creates many opportunities to advance electrochemical research. This ACES system allows deposition of diverse materials on various surfaces. High sulfur loading is necessary to compete with the current lithium-ion technology, and ACES offers potential to improve the total sulfur loading while maintaining high volumetric energy density. However, incorporation of the binder is paramount to adhere higher amount of active materials on the current collector. Therefore, modified conductive polymer binder is needed to optimize the lithium-sulfur performance.

4. Conclusion

The air-controlled electrospray process offers many benefits over the slurry casting method. The removal of binder, increased tortuosity, and improved pore mechanical structure enhance the electrical conductivity, electrolyte accessibility, and sulfur adsorption, which ultimately improves lithium-sulfur electrochemical performance. In addition, the elimination of a drying step avoids surface cracking and offers the potential for scaled up processes. An environmental issue is also mitigated by replacing common toxic organic solvent for sulfur deposition (N-Methyl-2-pyrrolidone or Carbon disulfide or chloroform) with more relatively benign solvent (80% water and 20% isopropanol). This novel system exhibits a potential for energy storage applications.

ACKNOWLEDGMENTS

This work was partly funded by the Battery 500 Seedling Program of the Energy Efficiency & Renewable (EERE) Office in U.S. Department of Energy (DE-EE0008193) and Axiom Nano, LLC (Cornell OSP No. 80674). All the material characterizations were obtained via facilities at the Cornell Center for Materials Research (part of NSF MRSEC Program, Grant DMR 1120296).

Supporting Information Available: FTIR spectra and High resolution S_{2p} before and after heat treatment, digital image of air-controlled electrospray setup, TGA of sulfur-carbon composite after the spray process, SEM images of sulfur cathode morphology prepared by SC, ACES, and ACES-Gr before and after cycling at different resolutions, SEM and EDS mapping of lithium metal from SC, ACES, and ACES-Gr after cycling.

References.

- (1) Urbonaite, S.; Poux, T.; Novák, P. Progress Towards Commercially Viable Li-S Battery Cells. *Adv. Energy Mater.* **2015**, *5*, 1500118.
- (2) Manthiram, A.; Chung, S.-H.; Zu, C. Lithium-Sulfur Batteries: Progress and Prospects. *Adv. Mater.* **2015**, *27*, 1980–2006.
- (3) Lochala, J.; Liu, D.; Wu, B.; Robinson, C.; Xiao, J. Research Progress toward the Practical Applications of Lithium–Sulfur Batteries. *ACS Appl. Mater. Interfaces* **2017**, *9*, 24407–24421.
- (4) Yin, Y. X.; Xin, S.; Guo, Y. G.; Wan, L. J. Lithium-Sulfur Batteries: Electrochemistry, Materials, and Prospects. *Angewandte Chemie - International Edition.* **2013**, *52*, 13186–13200.

- (5) Eroglu, D.; Zavadil, K. R.; Gallagher, K. G. Critical Link between Materials Chemistry and Cell-Level Design for High Energy Density and Low Cost Lithium-Sulfur Transportation Battery. *J. Electrochem. Soc.* **2015**, *162*, A982–A990.
- (6) Manthiram, A.; Fu, Y.; Su, Y.-S. Challenges and Prospects of Lithium-Sulfur Batteries. *Acc. Chem. Res.* **2013**, *46*, 1125-1134.
- (7) Manthiram, A.; Fu, Y.; Chung, S.-H.; Zu, C.; Su, Y.-S. Rechargeable Lithium–Sulfur Batteries. *Chem. Rev.* **2014**, *114*, 11751–11789.
- (8) Bresser, D.; Passerini, S.; Scrosati, B. Recent Progress and Remaining Challenges in Sulfur-Based Lithium Secondary Batteries--a Review. *Chem. Commun. (Camb)*. **2013**, *49*, 10545–10562.
- (9) He, G.; Ji, X.; Nazar, L. High “C” Rate Li-S Cathodes: Sulfur Imbibed Bimodal Porous Carbons. *Energy Environ. Sci.* **2011**, *4*, 2878.
- (10) Rao, M.; Song, X.; Cairns, E. J. Nano-Carbon/Sulfur Composite Cathode Materials with Carbon Nanofiber as Electrical Conductor for Advanced Secondary Lithium/Sulfur Cells. *J. Power Sources* **2012**, *205*, 474–478.
- (11) Song, J.; Xu, T.; Gordin, M. L.; Zhu, P.; Lv, D.; Jiang, Y. B.; Chen, Y.; Duan, Y.; Wang, D. Nitrogen-Doped Mesoporous Carbon Promoted Chemical Adsorption of Sulfur and Fabrication of High-Areal-Capacity Sulfur Cathode with Exceptional Cycling Stability for Lithium-Sulfur Batteries. *Adv. Funct. Mater.* **2014**, *24*, 1243–1250.
- (12) Guo, J.; Xu, Y.; Wang, C. Sulfur-Impregnated Disordered Carbon Nanotubes Cathode for Lithium-Sulfur Batteries. *Nano Lett.* **2011**, *11*, 4288–4294.
- (13) Barinov, A.; Gregoratti, L.; Dudin, P.; Rosa, S. La; Kiskinova, M. Imaging and Spectroscopy of Multiwalled Carbon Nanotubes during Oxidation: Defects and Oxygen

- Bonding. *Adv. Mater.* **2009**, *21*, 1916–1920.
- (14) Zhou, G.; Li, F.; Cheng, H.-M. Progress in Flexible Lithium Batteries and Future Prospects. *Energy Environ. Sci.* **2014**, *7*, 1307–1338.
- (15) Li, Q.; Zhang, Z.; Zhang, K.; Fang, J.; Lai, Y.; Li, J. A Simple Synthesis of Hollow Carbon Nanofiber-Sulfur Composite via Mixed-Solvent Process for Lithium-Sulfur Batteries. *J. Power Sources* **2014**, *256*, 137–144.
- (16) Lee, J.; Ko, B.; Kang, J.; Chung, Y.; Kim, Y.; Halim, W.; Lee, J. H.; Joo, Y. L. Facile and Scalable Fabrication of Highly Loaded Sulfur Cathodes and Lithium–sulfur Pouch Cells via Air-Controlled Electrospray. *Mater. Today Energy* **2017**, *6*, 255–263.
- (17) Williams, B. P.; Joo, Y. L. Tunable Large Mesopores in Carbon Nanofiber Interlayers for High-Rate Lithium Sulfur Batteries. *J. Electrochem. Soc.* **2016**, *163*, A2745–A2756.
- (18) Wang, J.; Yang, Y.; Kang, F. Porous Carbon Nanofiber Paper as an Effective Interlayer for High-Performance Lithium-Sulfur Batteries. *Electrochim. Acta* **2015**, *168*, 271–276.
- (19) Li, H.; Sun, M.; Zhang, T.; Fang, Y.; Wang, G. Improving the Performance of PEDOT-PSS Coated Sulfur@activated Porous Graphene Composite Cathodes for Lithium–sulfur Batteries. *J. Mater. Chem. A* **2014**, *2*, 18345–18352.
- (20) Gong, Z.; Wu, Q.; Wang, F.; Li, X.; Fan, X.; Yang, H.; Luo, Z. PEDOT-PSS Coated Sulfur/Carbon Composite on Porous Carbon Papers for High Sulfur Loading Lithium–sulfur Batteries. *RSC Adv.* **2015**, *5*, 96862–96869.
- (21) Ji, L.; Rao, M.; Zheng, H.; Zhang, L.; Li, Y.; Duan, W.; Guo, J.; Cairns, E. J.; Zhang, Y. Graphene Oxide as a Sulfur Immobilizer in High Performance Lithium/Sulfur Cells. *J. Am. Chem. Soc.* **2011**, *133*, 18522–18525.
- (22) Zhou, X.; Li, Y.; Ma, G.; Ma, Q.; Lei, Z. One-Step Solid-State Synthesis of Sulfur-

- Reduced Graphene Oxide Composite for Lithium-Sulfur Batteries. *J. Alloys Compd.* **2016**, *685*, 216–221.
- (23) Stankovich, S.; Dikin, D. A.; Piner, R. D.; Kohlhaas, K. A.; Kleinhammes, A.; Jia, Y.; Wu, Y.; Nguyen, S. B. T.; Ruoff, R. S. Synthesis of Graphene-Based Nanosheets via Chemical Reduction of Exfoliated Graphite Oxide. *Carbon N. Y.* **2007**, *45*, 1558–1565.
- (24) Schniepp, H. C.; Li, J. L.; McAllister, M. J.; Sai, H.; Herrera-Alonson, M.; Adamson, D. H.; Prud'homme, R. K.; Car, R.; Seville, D. A.; Aksay, I. A. Functionalized Single Graphene Sheets Derived from Splitting Graphite Oxide. *J. Phys. Chem. B* **2006**, *110*, 8535–8539.
- (25) Liang, X.; Hart, C.; Pang, Q.; Garsuch, A.; Weiss, T.; Nazar, L. F. A Highly Efficient Polysulfide Mediator for Lithium-Sulfur Batteries. *Nat. Commun.* **2015**, *6*, 5682.
- (26) Qie, L.; Manthiram, A. A Facile Layer-by-Layer Approach for High-Areal-Capacity Sulfur Cathodes. *Adv. Mater.* **2015**, *27*, 1694–1700.
- (27) Zhang, L.; Ji, L.; Glans, P.-A.; Zhang, Y.; Zhu, J.; Guo, J. Electronic Structure and Chemical Bonding of a Graphene Oxide–sulfur Nanocomposite for Use in Superior Performance Lithium–sulfur Cells. *Phys. Chem. Chem. Phys.* **2012**, *14*, 13670.
- (28) Ganguly, A.; Sharma, S.; Papakonstantinou, P.; Hamilton, J. Probing the Thermal Deoxygenation of Graphene Oxide Using High-Resolution in Situ X-Ray-Based Spectroscopies. *J. Phys. Chem. C* **2011**, *115*, 17009–17019.
- (29) Mattevi, C.; Eda, G.; Agnoli, S.; Miller, S.; Mkhoyan, K. A.; Celik, O.; Mastrogiovanni, D.; Granozzi, G.; Carfunkel, E.; Chhowalla, M. Evolution of Electrical, Chemical, and Structural Properties of Transparent and Conducting Chemically Derived Graphene Thin Films. *Adv. Funct. Mater.* **2009**, *19*, 2577–2583.
- (30) Liang, X.; Hart, C.; Pang, Q.; Garsuch, A.; Weiss, T.; Nazar, L. F. A Highly Efficient

- Polysulfide Mediator for Lithium–sulfur Batteries. *Nat. Commun.* **2015**, *6*, 5682.
- (31) Ren, P.-G.; Yan, D.-X.; Ji, X.; Chen, T.; Li, Z.-M. Temperature Dependence of Graphene Oxide Reduced by Hydrazine Hydrate. *Nanotechnology* **2011**, *22*, 055705.
- (32) Tang, H.; Yang, C.; Lin, Z.; Yang, Q.; Kang, F.; Wong, C. P. Electro spray-Deposition of Graphene Electrodes: A Simple Technique to Build High-Performance Supercapacitors. *Nanoscale* **2015**, *7*, 9133–9139.
- (33) Mustafa, M.; Awais, M. N.; Pooniah, G.; Choi, K. H.; Ko, J.; Doh, Y. H. Electro spray Deposition of a Graphene-Oxide Thin Film, Its Characterization and Investigation of Its Resistive Switching Performance. *J. Korean Phys. Soc.* **2012**, *61*, 470–475.
- (34) Polfus, J. M.; Løvvik, O. M.; Rørvik, P. M.; Bredesen, R. Nanocomposites of Few-Layer Graphene Oxide and Alumina by Density Functional Theory Calculations. *J. Eur. Ceram. Soc.* **2016**, *36*, 719–724.
- (35) Fei, L.; Yoo, S. H.; Villamayor, R. A. R.; Williams, B. P.; Gong, S. Y.; Park, S.; Shin, K.; Joo, Y. L. Graphene Oxide Involved Air-Controlled Electro spray for Uniform, Fast, Instantly Dry, and Binder-Free Electrode Fabrication. *ACS Appl. Mater. Interfaces* **2017**, *9*, 9738–9746.
- (36) Seh, Z. W.; Li, W.; Cha, J. J.; Zheng, G.; Yang, Y.; McDowell, M. T.; Hsu, P. C.; Cui, Y. Sulphur-TiO₂ Yolk-Shell Nanoarchitecture with Internal Void Space for Long-Cycle Lithium-Sulphur Batteries. *Nat. Commun.* **2013**, *4*, 1331.
- (37) Peled, E.; Goor, M.; Schektman, I.; Mukra, T.; Shoval, Y.; Golodnitsky, D. The Effect of Binders on the Performance and Degradation of the Lithium/Sulfur Battery Assembled in the Discharged State. *J. Electrochem. Soc.* **2017**, *164*, A5001–A5007.
- (38) Han, Z.-J.; Yamagiwa, K.; Yabuuchi, N.; Son, J.-Y.; Cui, Y.-T.; Oji, H.; Kogure, A.;

- Harada, T.; Ishikawa, S.; Aoki, Y. Electrochemical Lithiation Performance and Characterization of Silicon–graphite Composites with Lithium, Sodium, Potassium, and Ammonium Polyacrylate Binders. *Phys. Chem. Chem. Phys.* **2015**, *17*, 3783–3795.
- (39) Ji, X.; Lee, K. T.; Nazar, L. F. A Highly Ordered Nanostructured Carbon–sulphur Cathode for Lithium–sulphur Batteries. *Nat. Mater.* **2009**, *8*, 500–506.
- (40) Schuster, J.; He, G.; Mandlmeier, B.; Yim, T.; Lee, K. T.; Bein, T.; Nazar, L. F. Spherical Ordered Mesoporous Carbon Nanoparticles with High Porosity for Lithium-Sulfur Batteries. *Angew. Chemie - Int. Ed.* **2012**, *51*, 3591–3595.
- (41) Pang, Q.; Kundu, D.; Cuisinier, M.; Nazar, L. F. Surface-Enhanced Redox Chemistry of Polysulphides on a Metallic and Polar Host for Lithium-Sulphur Batteries. *Nat. Commun.* **2014**, *5*, 4759.
- (42) Stobinski, L.; Lesiak, B.; Malolepszy, A.; Mazurkiewicz, M.; Mierzwa, B.; Zemek, J.; Jiricek, P.; Bieloshapka, I. Graphene Oxide and Reduced Graphene Oxide Studied by the XRD, TEM and Electron Spectroscopy Methods. *J. Electron Spectros. Relat. Phenomena* **2014**, *195*, 145–154.
- (43) Chen, H.; Müller, M. B.; Gilmore, K. J.; Wallace, G. G.; Li, D. Mechanically Strong, Electrically Conductive, and Biocompatible Graphene Paper. *Adv. Mater.* **2008**, *20*, 3557–3561.
- (44) Barai, P.; Mistry, A.; Mukherjee, P. P. Poromechanical Effect in the Lithium–sulfur Battery Cathode. *Extrem. Mech. Lett.* **2016**, *9*, 359–370.
- (45) Yamin, H.; Gorenshstein, A.; Penciner, J.; Sternberg, Y.; Peled, E. Lithium Sulfur Battery: Oxidation/Reduction Mechanism of Polysulfides in THF Solutions. *J. Electrochem. Soc.* **1988**, *135*, 1045.

- (46) Cheon, S.-E.; Ko, K.-S.; Cho, J.-H.; Kim, S.-W.; Chin, E.-Y.; Kim, H.-T. Rechargeable Lithium Sulfur Battery. *J. Electrochem. Soc.* **2003**, *150*, A800.
- (47) Akridge, J. R.; Mikhaylik, Y. V.; White, N. Li/S Fundamental Chemistry and Application to High-Performance Rechargeable Batteries. *Solid State Ionics*, **2004**, *175*, 243–245.
- (48) Kolosnitsyn, V. S.; Kuzmina, E. V.; Karaseva, E. V.; Mochalov, S. E. A Study of the Electrochemical Processes in Lithium-Sulphur Cells by Impedance Spectroscopy. *J. Power Sources* **2011**, *196*, 1478–1482.
- (49) Zhang, S. S. Improved Cyclability of Liquid Electrolyte Lithium/Sulfur Batteries by Optimizing Electrolyte/Sulfur Ratio. *Energies* **2012**, *5*, 5190-5197.
- (50) Li, N.; Zheng, M.; Lu, H.; Hu, Z.; Shen, C.; Chang, X.; Ji, G.; Cao, J.; Shi, Y. High-Rate Lithium-Sulfur Batteries Promoted by Reduced Graphene Oxide Coating. *Chem. Commun.* **2012**, *48*, 4106-4108.
- (51) Huang, J. Q.; Zhuang, T. Z.; Zhang, Q.; Peng, H. J.; Chen, C. M.; Wei, F. Permselective Graphene Oxide Membrane for Highly Stable and Anti-Self-Discharge Lithium-Sulfur Batteries. *ACS Nano* **2015**, *9*, 3002–3011.
- (52) Fantauzzi, M.; Elsener, B.; Atzei, D.; Rigoldi, A.; Rossi, A. Exploiting XPS for the Identification of Sulfides and Polysulfides. *RSC Adv.* **2015**, *5*, 75953–75963.
- (53) Fu, C.; Wong, B. M.; Bozhilov, K. N.; Guo, J. Solid State Lithiation–delithiation of Sulphur in Sub-Nano Confinement: A New Concept for Designing Lithium–sulphur Batteries. *Chem. Sci.* **2016**, *7*, 1224–1232.

